Microfluidics and Nanofluidics (2019)
https://doi.org/10.1007/s10404-019-2295-x - Supplementary material

Optimised multi-stream microfluidic designs for controlled extensional deformation

Konstantinos Zografos · Simon J. Haward · Mónica S. N. Oliveira

Received: 4 June 2019/Accepted: 18 October 2019

1 T-junction optimised using an abrupt profile

In our optimisations presented in the main part of the paper, we have use a smoothed velocity profile as a target. Here we consider two cases using a target velocity profile without a smoothing region, which we call "abrupt" velocity profile: a standard TJ with a straight and unchanged bottom boundary; a TJ where the shape of the bottom boundary is also optimised and thus, is allowed to change generating a cavity region (Soulages et al., 2009). All optimisations have been performed for a Newtonian fluid considering creeping flow conditions (Re $\to$ 0) considering the abrupt target velocity profile expressed by Eq. 1 if $n_2 = 0$, shown in Fig. 1a. This profile results in an instantaneous step change in the strain-rate both at the start and the end of the desired region. Figure 1a presents the normalised velocity profiles along the centreline of the flow at the region of interest, for both optimised cases. The obtained shapes for the straight-bottom case and the optimised cavity case are shown in Fig. 1b and Fig. 1c, respectively. It can be seen that in both configurations the existence of a transition length is required, in order for the velocity to start increasing in a continuous manner. The standard case presents a similar behaviour to that produced by the hyperbolic shape shown in Fig. 4 of Section 4.1.1, exhibiting a strain-rate overshoot, since the velocity cannot increase suddenly to the desired value. The abrupt velocity profile considered as target is inherently challenging both at the beginning and at the end of the desired constant strain-rate region. To tackle the challenges associated with the non-continuous velocity gradient at the start of the homogeneous desired strain-rate region, where changes are rapid, a T-junction where the cavity is optimised can be considered alternatively. It can be seen that the presence of the bottom cavity significantly reduces the strength of the overshoot, since the velocity is allowed to develop smoothly along a transition region. This smoother development of the velocity affects the final generated shape where the boundary deformations are less steep.

K. Zografos
School of Engineering, University of Liverpool, Brownlow Street, Liverpool L69 3GH, UK
E-mail: k.zografos@liv.ac.uk

K. Zografos · M. S. N. Oliveira
James Weir Fluids Laboratory, Department of Mechanical and Aerospace Engineering, University of Strathclyde, Glasgow G1 1XJ, UK

S. J. Haward
Okinawa Institute of Science and Technology Graduate University, Onna, Okinawa 904-0495, Japan

2 Performance of the 2D optimised TJ for different aspect ratios

The optimised shape for a 2D TJ discussed in Section IV A 2 (c.f. Fig. 6), will not necessarily perform ideally for 3D geometries since the kinematics of each geometry strongly depend from the value of the aspect ratio used. Figure 2 illustrates the performance of the 2D shape for various aspect ratios in the range $0.5 \leq \mathrm{AR} \leq 10$. It can be seen that for the case of $\mathrm{AR} = 10$ the strain-rate profile is well approximated. However, when the depth of the device starts to decrease and becomes smaller than the width, the strain-rate profile will not obtain the desired behaviour and thus, the 2D shape should not be used.

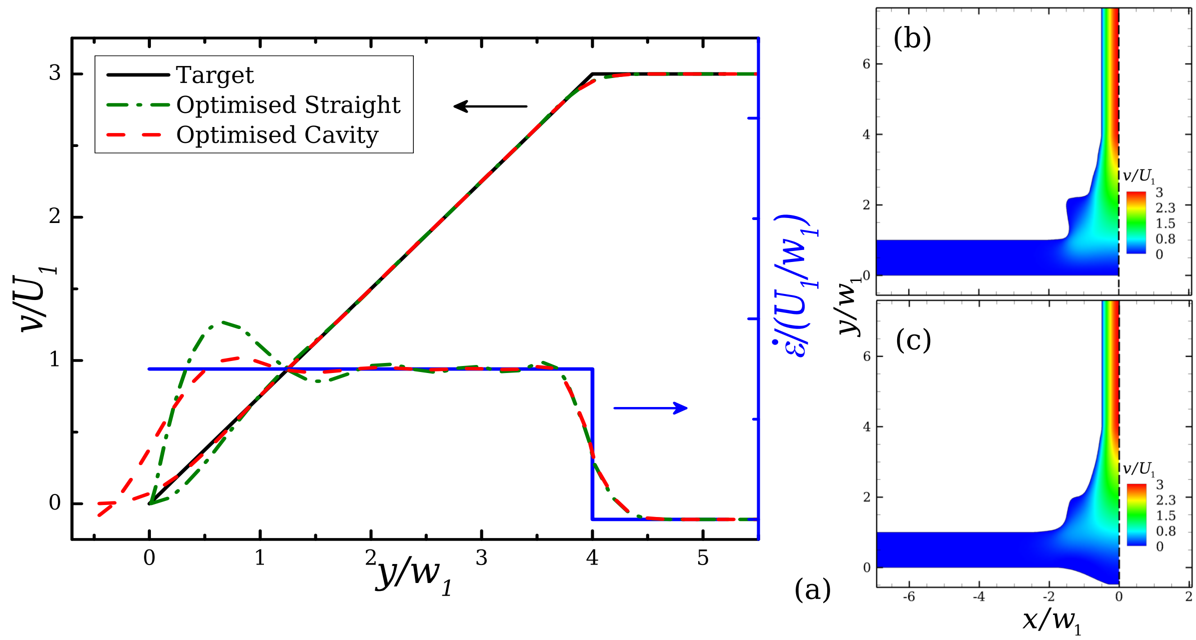

Fig. 1 Performance and shapes of the optimised 2D TJ designs using an abrupt profile (c.f. Eq.1 and Eq.2 for $n_2 = 0$): (a) Normalised velocity and strain-rate profiles along the centreline of the flow in the region of interest ($L_{\text{opt}} = 4w_1$) and contour-plots of the normalised y- velocity component for (b) the straight design and (c) the optimised cavity design. The *dashed* straight line in (b) and (c) illustrates the position of the symmetry axis and the flow centreline.

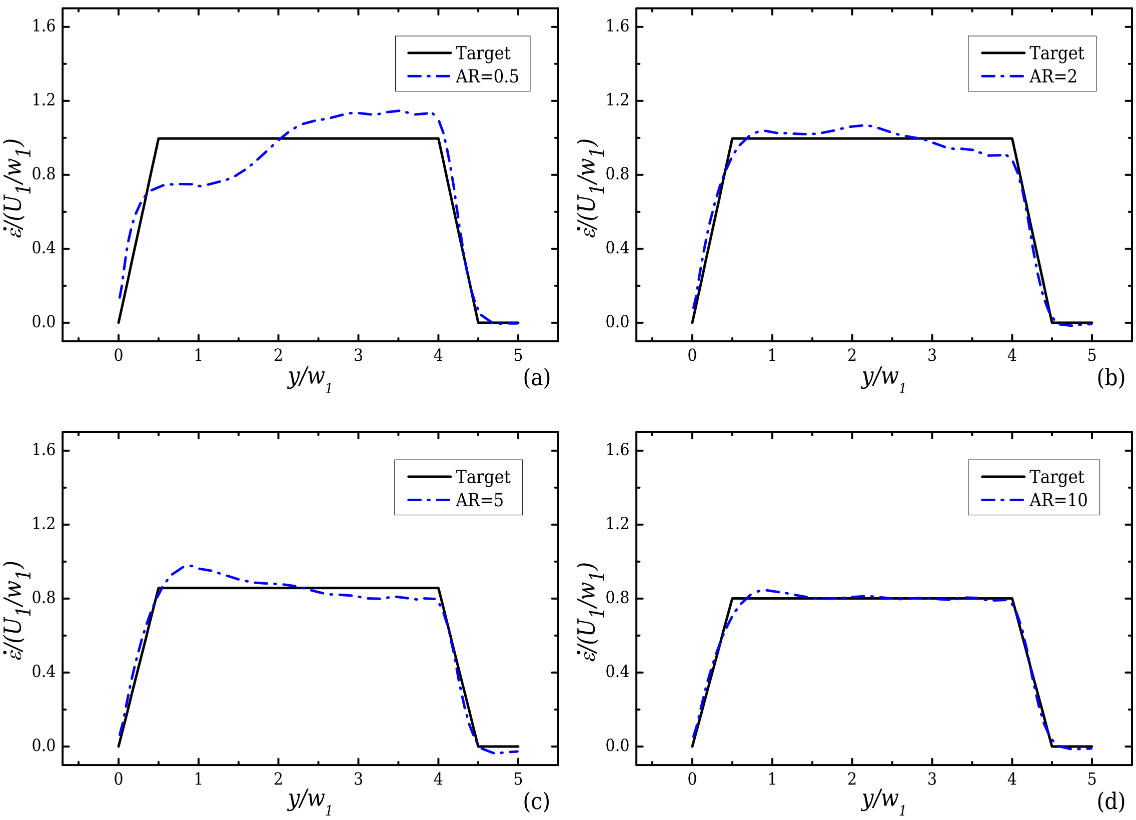

Fig. 2 Effect of the aspect ratio ($\text{AR} = w_1/d$) on the strain-rate profile computed along the flow centreline. The 3D geometries are designed using the 2D optimised shape for $\text{AR} = 0.5, 2, 5$ and 10 with $\text{WR} = 1$, $L_{\perp} = 4w_1$ and $l_{\varepsilon} = 0.5w_1$ considering creeping flow conditions.

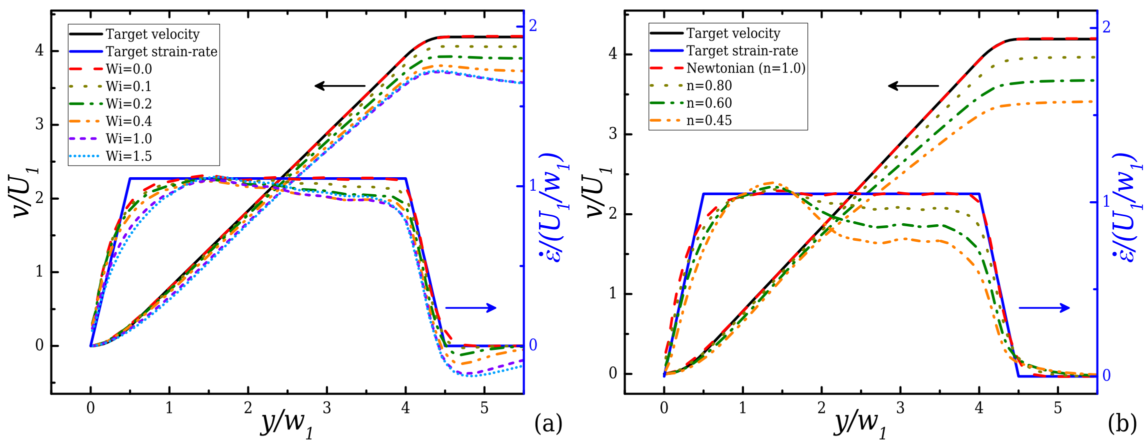

Fig. 3 Effects of rheological properties on the developed velocity and strain-rate profiles in the 3D optimised TJ design for the (a) sPTT at increasing Wi and (b) power-law model for different indices.

3 Shear thinning effect

In order to quantify the rheological effects for the flow of a shear-thinning fluid in the absence of elasticity within the optimised TJ and FF geometries, we employed the inelastic power-law model (Bird et al., 1987; Morrison, 2001) that can predict the variation of viscosity with the imposed shear-rate. For the power-law model the shear dependent viscosity is given as a function of the magnitude of the shear rate tensor:

$$\eta(\dot{\gamma}) = k\dot{\gamma}^{n-1} \qquad (1)$$

where k is the consistency index that is related to the magnitude of the viscosity and n is the power-law index. When $n = 1$, the Newtonian behaviour is recovered, predicting constant viscosity in steady shear. For $n < 1$, the fluid is described as shear-thinning, with the viscosity decreasing for increasing shear rate, while for $n > 1$ the fluid is described as shear-thickening with the fluid becoming more viscous as the deformation rate is increased.

Figures 3 and 4 demonstrate a comparison between the results presented in the original manuscript for the sPTT and those obtained for the power-law model within the 3D TJ and FF optimised designs respectively. In contrast with the data presented in the original manuscript, here the normalisation follows the standard approach in order for the shear-thinning behaviour to be visible both in the velocity and the strain-rate profiles. These results demonstrate that the behaviour deviates from the target for fluids with higher levels of shear-thinning (c.f. Fig. 3 for the TJ design and Fig. 4 for the FF design). Similarly to what is discussed in the main text, for both geometries it is clear that although the velocity at the outlet decreases due to the shear-thinning, a velocity overshoot close to the end of the optimised

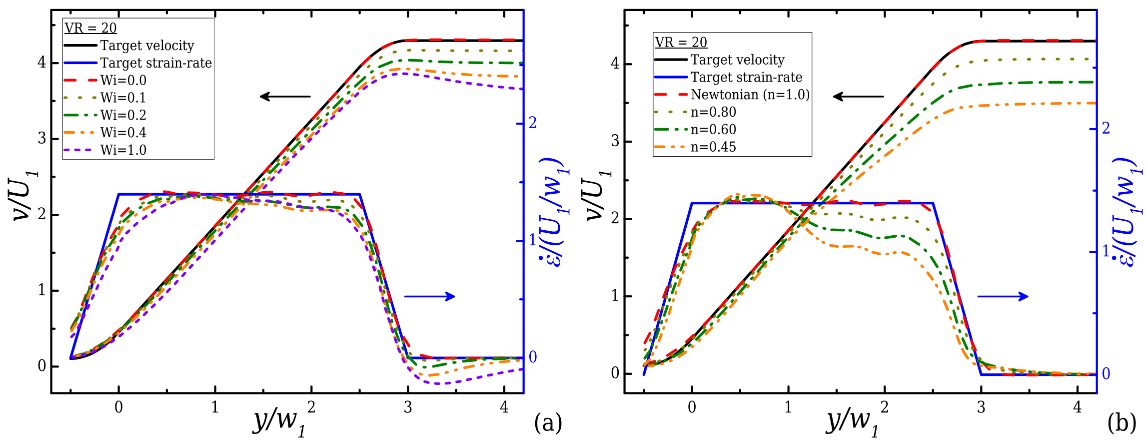

Fig. 4 Effects of rheological properties on the developed velocity and strain-rate profiles in the 3D optimised FF for VR = 20 design for the (a) sPTT at increasing Wi and (b) power-law model for different indices.

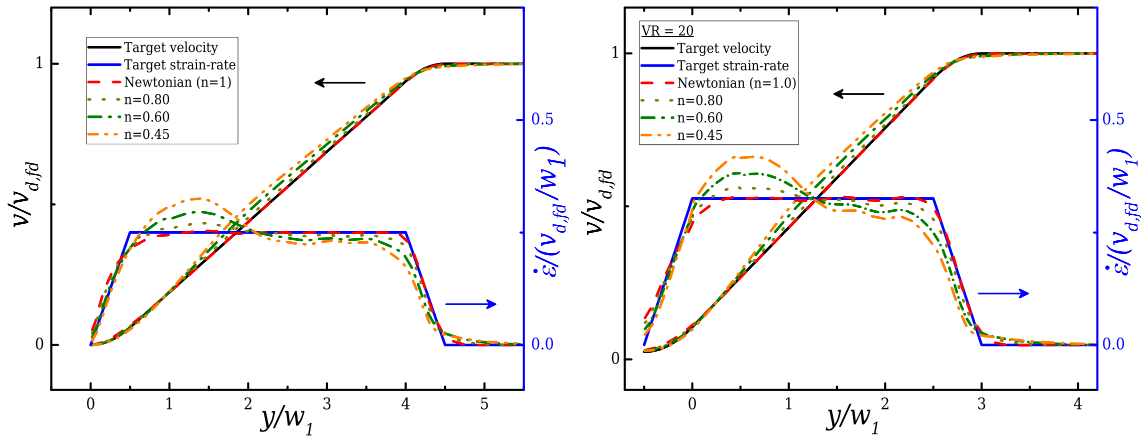

Fig. 5 Velocity and the resulted strain rate profiles along the flow centreline, normalised using the same approach as in the original manuscript (ν has been normalised with $\nu_{d,\mathrm{fd}}$) for the a power-law model within the (a) TJ and (b) FF optimised geometries.

region starts to become visible with increasing elasticity (c.f. Fig. 3a for the TJ design and Fig. 4a for the FF design). This overshoot is translated to an increasing undershoot of the strain-rates with increasing Wi. Obviously, these effects are not appearing for any of the inelastic cases examined with the power-law model (c.f. Fig. 3b for the TJ design and Fig. 4b for the FF design).

In order to be consistent with the normalisation used to present the results in the main part of the manuscript (Fig. 8b and Fig. 14b for the sPTT in a 3D optimised TJ and FF respectively), the obtained profiles for the inelastic shear-thinning fluids are also shown in Fig. 5 using the same approach (normalising with $\nu_{d,\mathrm{fd}}$). It can be seen that the higher the shear-thinning (decreasing n), the more enhanced the overshoot of the strain-rates becomes in both designs. A similar result was also predicted in Pimenta et al. (2018) for their optimised designs.

References

Bird RB, Armstrong RC, Hassager O (1987) Dynamics of Polymeric Liquids. Volume 1: Fluid Dynamics. John Wiley & Sons, New York

Morrison FA (2001) Understanding Rheology. Oxford University Press, Inc.

Pimenta F, Sousa RG, Alves MA (2018) Optimization of flow-focusing devices for homogeneous extensional flow. Biomicrofluidics 12(054103), DOI 10.1063/1.5037472

Soulages J, Oliveira MSN, Sousa PC, Alves MA, McKinley GH (2009) Investigating the stability of viscoelastic stagnation flows in T-shaped microchannels. J non-Newtonian Fluid Mech 163:9–24, DOI 10.1016/j.jnnfm.2009.06.002